We are IntechOpen,
the world's leading publisher of
Open Access books
Built by scientists, for scientists

6,900
Open access books available

185,000
International authors and editors

200M
Downloads

154
Countries delivered to

Our authors are among the

TOP 1%
most cited scientists

12.2%
Contributors from top 500 universities

CLARIVATE ANALYTICS
BOOK CITATION INDEX
INDEXED

WEB OF SCIENCE™

Selection of our books indexed in the Book Citation Index
in Web of Science™ Core Collection (BKCI)

Interested in publishing with us?
Contact book.department@intechopen.com

Band Structure and Magneto- Transport Properties in II-VI Nanostructures Semiconductors - Application to Infrared Detector Superlattices

Abdelhakim Nafidi

Laboratory of Condensed Matter Physics and Nanomaterials for Renewable Energy
University Ibn-Zohr,
Agadir
Morocco

1. Introduction

To observe phenomena by the image through invisible radiation to the eye is probably doubtless an old dream of humanity. The way followed to observe the invisible is to study an artificial retina constituted by a matrix of elements sensitive to radiation and to associate it with a system of acquisition and data processing. In brief a camera or a digital camera sensitive to other radiations than the visible light. The detectors are constituted of simple elementary p - n junctions realized in a semiconductor material whose height band gap is adapted to the energy of infrared photons which we wish to detect.

The work of (Essaki & Tsu, 1970) caused a big interest to the study of superlattices made from alternating layers of two semiconductors. The development of molecular beam epitaxy (MBE) was successfully applied to fabricate different quantum wells and superlattices. Among them III-V superlattices [$Ga_{1-x}Al_xAs$-GaAs (Essaki & Tsu, 1970) – (Dingle et al., 1975) - type I], IV-IV [InAs/GaSb (Sakaki et al, 1978) - type II] and later II-IV superlattice [HgTe/CdTe (Bastard, 1982) - type III]. The later is a stable alternative for application in infrared optoelectronic devices than the $Hg_{1-x}Cd_xTe$ alloys. Especially in the region of second atmospheric window (around 10 µm) which is of great interest for communication.

HgTe and CdTe crystallize in zinc –blend lattice respectively. The lattice-matching within 0.3 % yield to a small interdiffusion between HgTe and CdTe layers at low temperature near 200 °C by MBE. HgTe is a zero gap semiconductor (due to the inversion of relative positions of Γ_6 and Γ_8 edges (Tuchendler et al, 1973)) when it is sandwiched between the wide gap semiconductor CdTe (1.6 eV at 4.2 K) layers yield to a small gap HgTe/CdTe superlattice which is the key of an infrared detector.

A number of papers have been published devoted to the band structure of this system (Bastard, 1982) as well as its magnetooptical and transport properties (Nafidi, 2002). The aim of this work is to show the correlation between calculated bands structures and magneto-transport properties in two HgTe/CdTe nanostructures superlattices.

Our calculations of the specters of energy $E(d_2)$, $E(k_z)$ and $E(k_p)$, respectively, in the direction of growth and in plane of the superlattice;were performed in the envelope function formalism. Our two samples are denoted SL1 and SL2.

In the SL1, X-ray diffraction, conductivity, Hall effect, Seebek and Shubnikov-de Haas effects and angular dependence of the transverse magnetoresistance were measured. The profile of the (222) Bragg reflection indicated a modulated structure. At 4.2 K, the sample exhibits p type conductivity with a Hall mobility of 8200 cm²/Vs. This allowed us to observe the Shubnikov-de Haas effect with $p = 1{,}80 \ 10^{12}$ cm⁻². Using the calculated effective mass ($m^*_{HH} = 0{,}297 \ m_0$) of the degenerated heavy holes gas, the Fermi energy (2D) was $E_F = 14$ meV in agreement with 12 meV of thermoelectric power α. In intrinsic regime, $\alpha \sim T^{-3/2}$ and R_H $T^{3/2}$ indicates a gap $E_g = E_1 - HH_1 = 190$ meV in agreement with calculated $E_g(\Gamma, 300 \ K) = 178$ meV. The formalism used here predicts that the system is semiconductor for $d_1/d_2 = 1{,}87$ and $d_2 < 150$ Å. Here, $d_2 = 30$ Å and $E_g (\Gamma, 4.2 \ K) = 111$ meV so this sample is a two-dimensional modulated nanostructure medium-infrared detector semiconductor ($7\mu m < \lambda < 11\mu m$).

In the SL2, the angular dependence of the transverse magnetoresistance follows the two-dimensional (2D) behaviour with Shubnikov-de Haas oscillations. While the hall voltage goes to zero when the field is parallel to the plane. At low temperature, the sample exhibits p type conductivity with a hole mobility of 900 cm²/V.s. A reversal the sign of the weak-field Hall coefficient occurs at 25 K with an electron mobility of 3.10^4 cm²/Vs. In intrinsic regime, the measured $E_g \approx 38$ meV agree with calculated $E_g(\Gamma, 300K) = 34$ meV witch coincide with the Fermi level energy. The formalism used here predicts that the system is semi metallic for $d_1/d_2 = 4.1$ and $d_2 \geq 30$ Å. In our case $d_2 = 44$ Å and the gap $E_g(\Gamma, 4.2 \ K) = 3$ meV. In spite of it, this sample exhibits a semi metallic p type conduction mechanism, with a quasi-two-dimensional behavior and is a far-infrared detector (50 µm< λ< 450 µm). The investigated thicknesses of the SL2 situate it at the semiconductor to semimetal electronic transition.

In conclusion, we will show that the HgTe/CdTe nano-superlattice is a stable alternative for application in infrared optoelectronic devices than the alloys $Hg_{1-x}Cd_xTe$.

2. Experimental techniques

Our two HgTe/CdTe superlattices samples SL1 and SL2, grown by molecular beam epitaxy (MBE) on a CdTe (111) substrate at 180 °C, had a period $d = d_1 + d_2$ (90 layers) of HgTe ($d_1 = 5{,}6$ nm) / CdTe ($d_2 = 3$ nm) and (100 layers) of HgTe ($d_1 = 18$ nm) / CdTe ($d_2 = 4.4$ nm) respectively. Each sample was cut from an epitaxial wafer with a typical size of 5×1×1 mm³. The ohmic contacts were obtained by chemical deposition of gold from a solution of tetrachloroauric acid in methanol after a proper masking to form the Hall crossbar. Carriers transport properties were studied in the temperature range 1.5-300K in magnetic field up to 17 Tesla. Conductivity, Hall Effect, Seebek effect, X-ray diffraction and angular dependence of the transverse magnetoresistance were measured. The measurements at weak magnetic fields (up to 1.2 T) were performed into standard cryostat equipment. The measurements of the magnetoresistance were done under a higher magnetic field (up to 17 T), the samples were immersed in a liquid helium bath, in the center of a superconducting coil. Rotating samples with respect to the magnetic field direction allowed one to study the angular dependence of the magnetoresistance.

Band Structure and Magneto- Transport Properties in II-VI Nanostructures
Semiconductors. Application to Infrared Detector Superlattices

285

3. Theory of structural bands

Calculations of the spectra of energy E (k_z) and E(k_p), respectively, in the direction of growth and in plane of the superlattice; were performed in the envelope function formalism (Bastard, 1982) (Nafidi, 2002) with a valence band offset Λ between heavy holes bands edges of HgTe and CdTe of 40 meV determined by the magneto-optical absorption experiments (Guldner, 1984)

The general dispersion relation of the light particle (electron and light hole) subbands of the superlattice is given by the expression (Bastard, 1982) :

$$\cos k_z(d_1+d_2) = \cos (k_1 d_1) \cos (k_2 d_2) - \frac{1}{2}\left[\left(\xi+\frac{1}{\xi}\right)+\frac{k_p^2}{4k_1 k_2}\left(r+\frac{1}{r}-2\right)\right]\sin(k_1 d_1)\sin(k_2 d_2) \quad (1)$$

where the subscripts 1 and 2 refer to HgTe and CdTe respectively. k_z is the superlattice wave vector in the direction parallel to the growth axis z. The two-dimensional wave vector $k_p(k_x,k_y)$ describes the motion of particles perpendicular to k_z. Here,

$$\xi = \frac{k_1}{k_2} r \text{ , and } r = \frac{E - \varepsilon_2}{E + |\varepsilon_1| - \Lambda} \quad (2)$$

E is the energy of the light particle in the superlattice measured from the top of the Γ_8 valence band of bulk CdTe, while εi (i =1 or 2) is the interaction band gaps $E(\Gamma_6) - E(\Gamma_8)$ in the bulk HgTe and CdTe respectively. At given energy, the two–band Kane model (Kane, 1957).gives the wave vector ($k_i^2+k_p^2$) in each host material:

$$\left.\begin{array}{ll} \dfrac{2}{3} P^2 \hbar^2 (k_1^2 + k_p^2) = (E-\Lambda)(E - \Lambda + |\varepsilon_1|) & \text{for HgTe} \\[4mm] \dfrac{2}{3} P^2 \hbar^2 (k_2^2 + k_p^2) = E(E - \varepsilon_2) & \text{for CdTe} \end{array}\right\} \quad (3)$$

P is the Kane matrix element given by the relation:

$$\frac{2P^2}{3|\varepsilon_1|} = \frac{1}{2m^*} \quad (4)$$

where $m^* = 0.03 m_0$ is the electron cyclotron mass in HgTe (Tuchendler et al, 1973). For a given energy E, a superlattice state exists if the right-hand side of Eq. (1) lies in the range [-1,1]. That implies $-\pi/d \leq k_z \leq -\pi/d$ in the first Brillion zone.

The heavy hole subbands of the superlattice are given by the same Eq. (1) with :

$$\xi = \frac{k_1}{k_2}r, \text{ and } r = 1 \text{ with}\left\{\begin{array}{ll} -\dfrac{\hbar^2(k_1^2+k_p^2)}{2 m^*_{HH}} = E - \Lambda & \text{for HgTe} \\[4mm] -\dfrac{\hbar^2(k_2^2+k_p^2)}{2 m^*_{HH}} = E & \text{for CdTe} \end{array}\right. \quad (5)$$

m*$_{HH}$ =0.3 m$_0$ (Tuchendler et al, 1973) is the effective heavy hole mass in the host materials. The band structure computation consists of solving Eq. (1) which represents the dispersion relations (i.e. finding the values of energy E which are roots of the Eq. (1) for a given value of the carrier wave vector). Here, we are interested in studying the states of energy of light particles and heavy holes in HgTe/CdTe superlattice as function of k$_z$ when k$_p$=0 and as function of k$_p$ when k$_z$=0 and when k$_z$=π/d. The solving procedure used for studying E as function k$_z$ in the case where k$_p$=0 consists of going, with a steep δE, through the studied range of energy E and then finding, for each value of E, the value of k$_z$ which satisfies the dispersion relations. The same procedure is used for studying E as function k$_p$ in the case where k$_z$=0 and k$_z$=π/d. It is noteworthy that, for a given value of E, Eq. (1) may have more than one root in k$_p$. It appears, from Eq. (3)-(5), that the carrier wave vectors k$_1$, k$_2$, and k$_p$ are either real or imaginary (i.e. complex) and then using complex numbers in the calculation seems to be more adequate.

4. The SL1: HgTe(d$_1$ = 5,6 nm) / CdTe(d$_2$ = 3 nm)

4.1 Theoretical results and discussions¶

The energy E as a function of d$_2$, at 4.2 K, in the center Γ of the first Brillouin zone and for our d$_1$ = 1.87 d$_2$, is shown in Fig. 1. (a) (El Abidi et al, 2010). The case of our sample (d$_2$ = 30 Å) is indicated by the vertical broken line. Here the cross-over of E$_1$ and HH$_1$ subbands occurs. d$_2$ controls the superlattice band gap E$_g$=EE$_1$-E$_{HH1}$. For weak d$_2$ the sample is semiconductor with a strong coupling between the HgTe wells as in the SL1. At the dot T(d$_2$ = 150 Å, E= 39 meV) the gap goes to zero with the transition semiconductor- semimetal. When d$_2$ increases, E$_1$ and h$_1$ states drops in the energy gap [0, Λ] and become interface state with energy

$$E_I = \frac{\Lambda \varepsilon_2}{|\varepsilon_1| + \varepsilon_2} = 34 \text{ meV} \tag{6}$$

for infinite d$_2$ obtained from Eq. (1). Then the superlattice has the tendency to become a layer group of isolated HgTe wells and thus assumes a semimetallic character. The ratio d$_1$/d$_2$ governs the width of superlattice subbands (i.e. the electron effective mass). A big d$_1$/d$_2$, of 4.09 as in the case of the SL2, moves away the material from the two-dimensional behavior.

In the Fig. 1. (b) we can see that the band gap E$_g$(Γ) increases, presents a maximum at 40 meV and decreases when the valence band offset Λ between heavy hole band edges of HgTe and CdTe increase. For each Λ, E$_g$(Γ) increases with T. Our chosen value of 40 meV is indicated by a vertical dashed line. This offset agrees well with our experimental results contrary to 0 meV used by (Bastard, 1982) and 360 meV given by (Johnson et al, 1988). The later offset give E$_g$ (300 K) =135 meV in the right of Fig. 1 whereas, in intrinsic regime, α ~T$^{-3/2}$ and R$_H$ T$^{3/2}$ indicates a measured gap E$_g$ ≈ 190 meV in agreement with calculated E$_g$(Γ,300 K) = 178 meV.

Fig. 2 shows that, for each d$_2$, E$_g$ (Γ) decreases when d$_1$/d$_2$ increases. For each d$_1$/d$_2$, when d$_2$ increases E$_g$ (Γ) decreases, go to zero at the transition dot T and became negative for a semimetal conductivity. In the right of Fig. 2, the cut-off wavelength |λ$_c$| diverge at T with d$_2$=54 Å, 100 Å, 150 Å,… respectively for d$_1$/d$_2$=4.09, 2.67, 1.87, … Thus, the transition goes to high d$_2$ when d$_1$/d$_2$ decreases. In the case of our samples the transition occurs, respectively, at d$_2$ =150 Å and 54 Å in the SL1 and the SL2.

Band Structure and Magneto- Transport Properties in II-VI Nanostructures
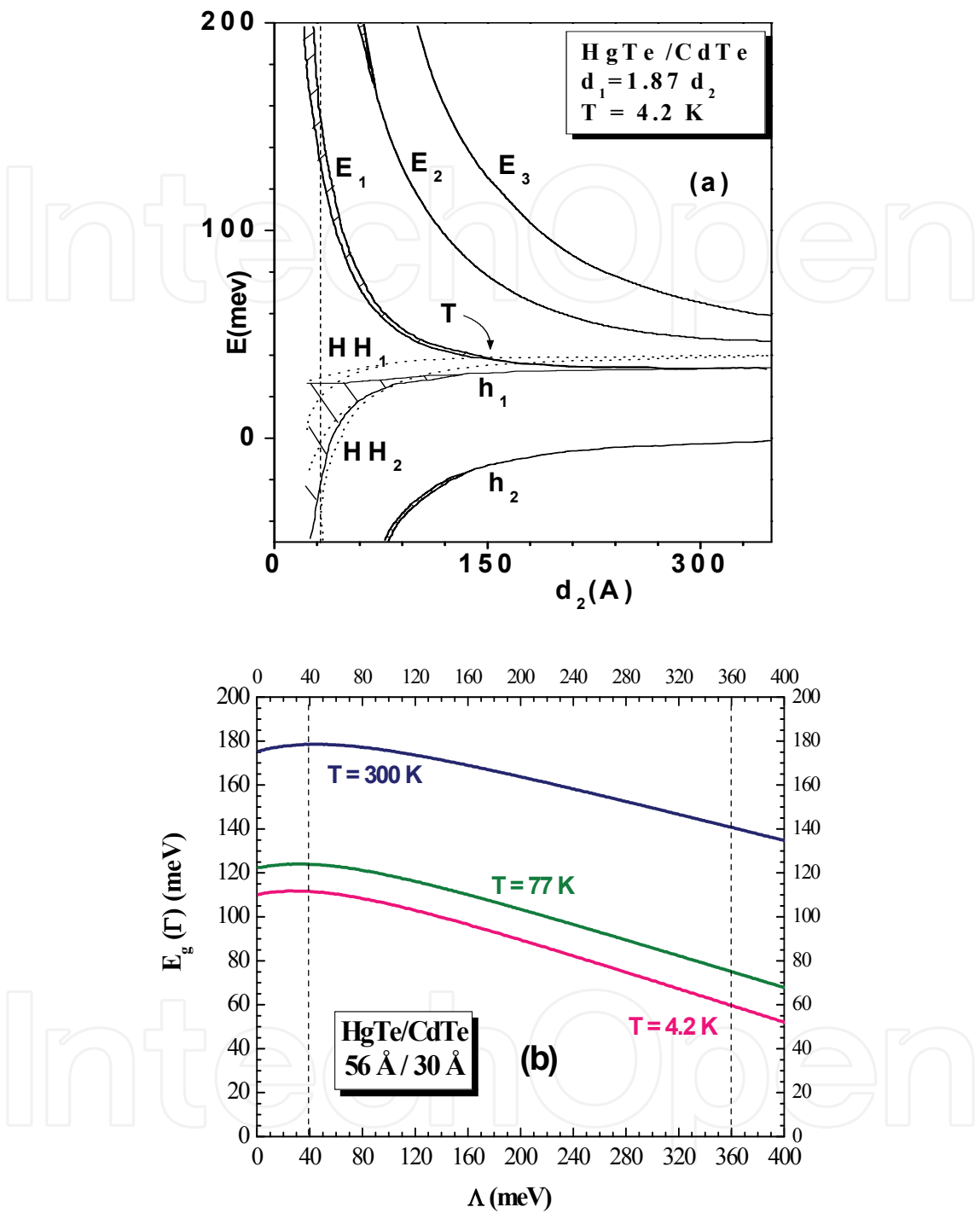Semiconductors. Application to Infrared Detector Superlattices

287

Fig. 1. (a) Energy position and width of the conduction (E_i), heavy-hole (HH_i), and the light-hole (h_1) subbands calculated at 4,2 K in the center Γ of the first Brillouin zone as a function of layer thickness d_2 for HgTe/CdTe superlattice with $d_1 = 1.87\ d_2$, where d_1 and d_2 are the thicknesses of the HgTe and CdTe layers, respectively. T is the point of the transition semiconductor- semimetal. (b) the band gap $E_g\ (\Gamma)$, in the center Γ of the first Brillouin zone, as function of temperature and valence band offset Λ between heavy holes bands edges of HgTe and CdTe for the investigated HgTe/CdTe superlattice
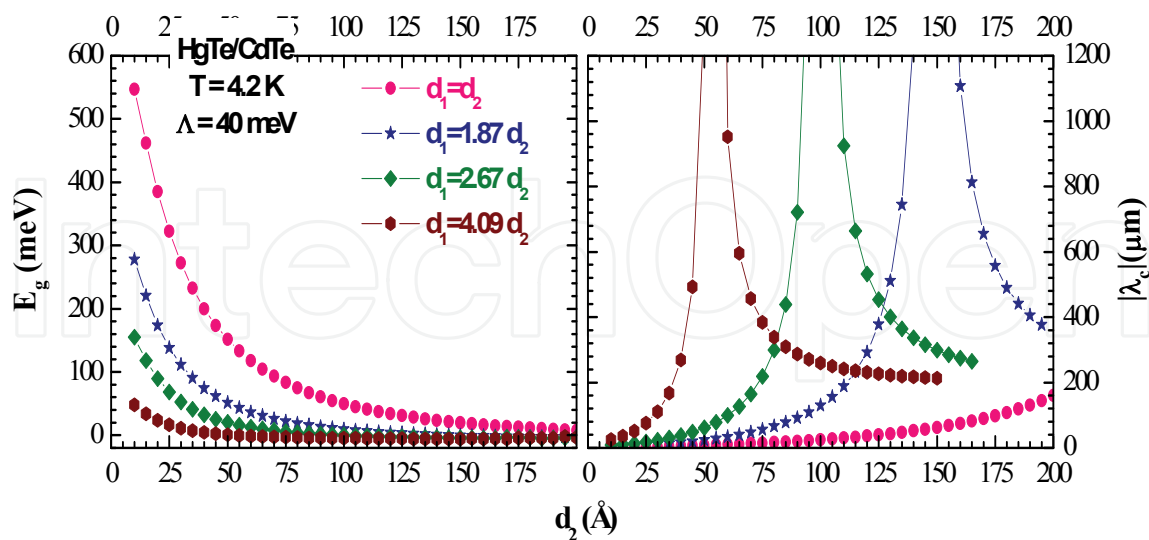
Fig. 2. E_g (Γ) and $|\lambda c|$ as function of d_2 for various d_1/d_2 at 4.2 K
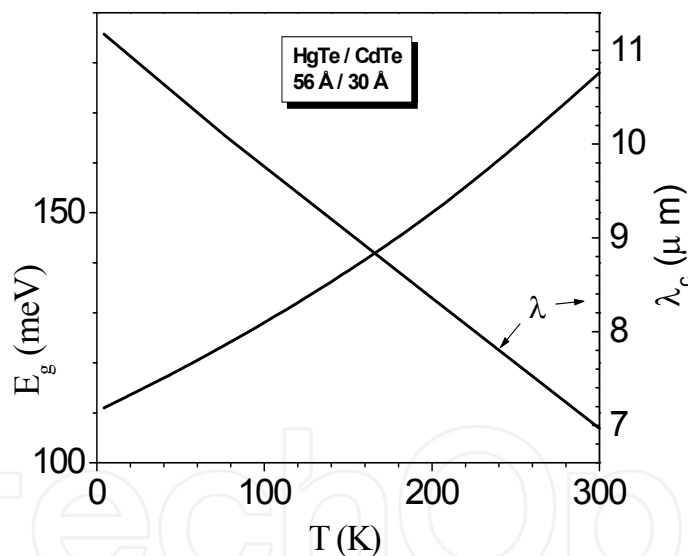

Fig. 3. Temperature dependence of the band gap E_g and the cut-off wavelength λ_c, at the center Γ of the first Brillouin zone

Using the value of the gaps ε_1 and ε_2 at different temperatures between 4.2 K and 300 K (Weiler, 1981) and taking P temperature independent, this is supported by the fact that from Eq. (4) $P \approx \varepsilon_i(T)/m^*(T) \approx cte$, we get the temperature dependence of the band gap E_g, in the center Γ of the first Brillouin zone in Fig. 3. Note that E_g increases from 111 meV at 4.2 K to 178 meV at 300K. We calculated the detection cut-off wave length by the relation

$$\lambda_c(\mu m) = \frac{1240}{E_g(meV)} \tag{7}$$

Band Structure and Magneto- Transport Properties in II-VI Nanostructures
Semiconductors. Application to Infrared Detector Superlattices

289

In the investigated temperature range 7 μm< λ <11 μm situates our sample as a medium infrared detector.

In Fig. 4 we can see the specters of energy $E(k_z)$ and $E(k_p)$, respectively, in the direction of growth and in plane of the superlattice at 4.2 K. Along k_z the subbands E_1 and h_1 are wide and non-parabolic. Along k_p, E_1 and h_1 increase with k_p whereas HH_n decreases. This yield
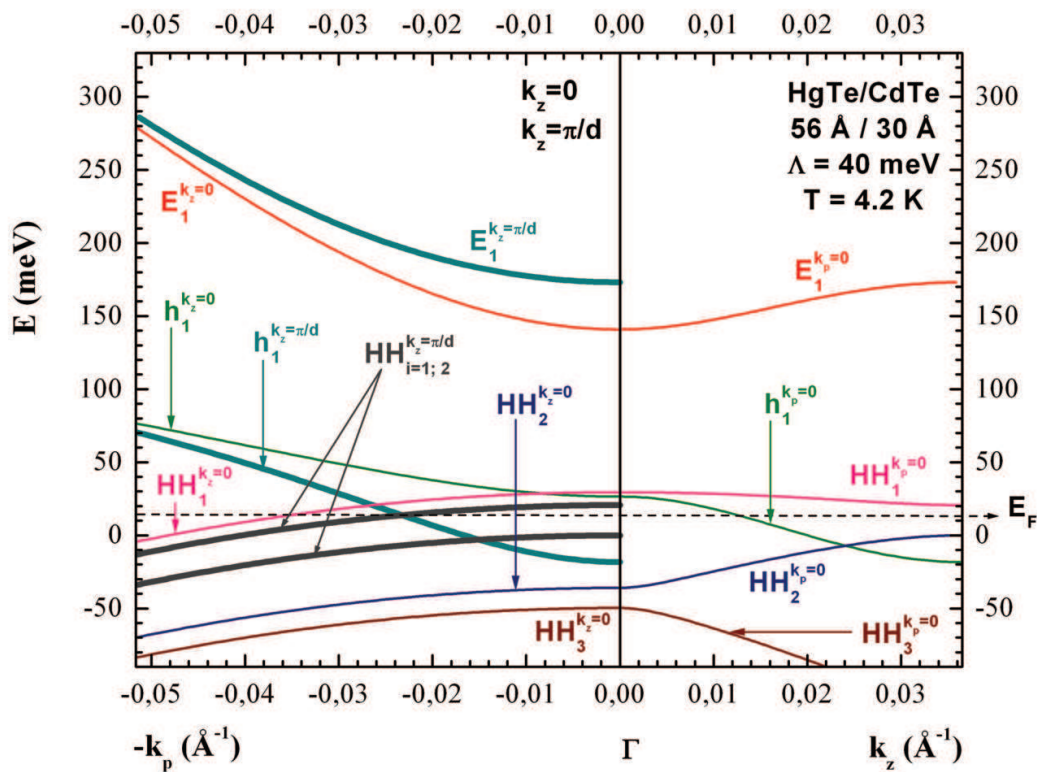
Fig. 4. Calculated bands along the wave vector k_z in the right and in plane $k_p(k_x,k_y)$ in the left, of the HgTe/CdTe superlattice at 4.2 K. E_F is the energy of Fermi level

to an anti-crossing of HH_1 and h_1 at k_p= 0.01 Å⁻¹ corresponding to a magnetic field of 4 Teslas according to the Formula (13).

4.2 Experimental results and discussions

In Fig. 2, $|\lambda c|$ as function of d_2, at 4.2 K, shows that there is a multiple choice of d_2 for medium infrared detectors with $|\lambda c| \leq$ 10μm for each d_1/d_2. Our choice of d_2= 3 nm for d_1=1.87 d_2 give a calculated $E_g(\Gamma,300 K)$ = 178 meV corresponding to E_g (Γ, 300 K) =183 meV for the well used random alloys $Hg_{0.8}Cd_{0.2}Te$ (Hansen et al, 1982).

In Fig. 5(a) we can see that the angular dependence of the transverse magnetoresistance vanishes, when the field is parallel to the plane of the SL, indicating a two dimensional (2D) behavior confirmed by the observation of SDH oscillations in Fig. 7(a).

At low temperatures, the sample exhibits p type conductivity (confirmed by our thermoelectric power measurements in Fig. 6(b)) with a concentration p=1.84 10^{12} cm⁻² and a Hall mobility μ_p = 8200 cm²/Vs in Fig. 5(b) (Nafidi et al, 2004). The decrease of R_H (1/T) at 55 K shown by arrow in Fig. 5(c) can be due to coupling between HgTe well (small d_1/d_2 and d_2), to the widening of carrier sub-bands under the influence of the magnetic field
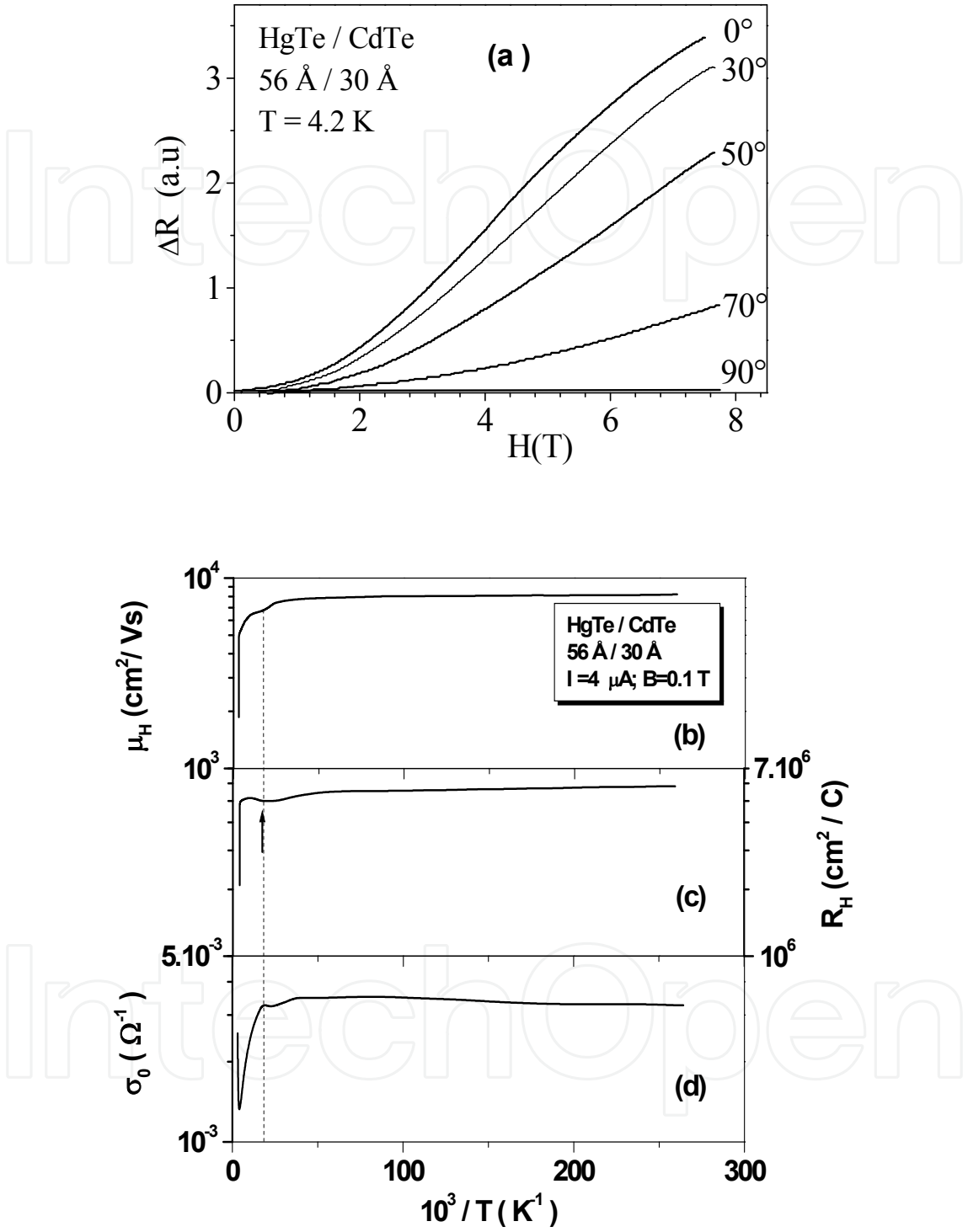
Fig. 5. (a) Variation of magnetoresistance of the sample with various angles between the magnetic field and the normal to the HgTe/CdTe superlattice surface. Temperature dependence of the Hall mobility (b), weak-field Hall coefficient (c) and conductivity (d) (Nafidi et al, 2002) in the investigated HgTe/CdTe superlattice
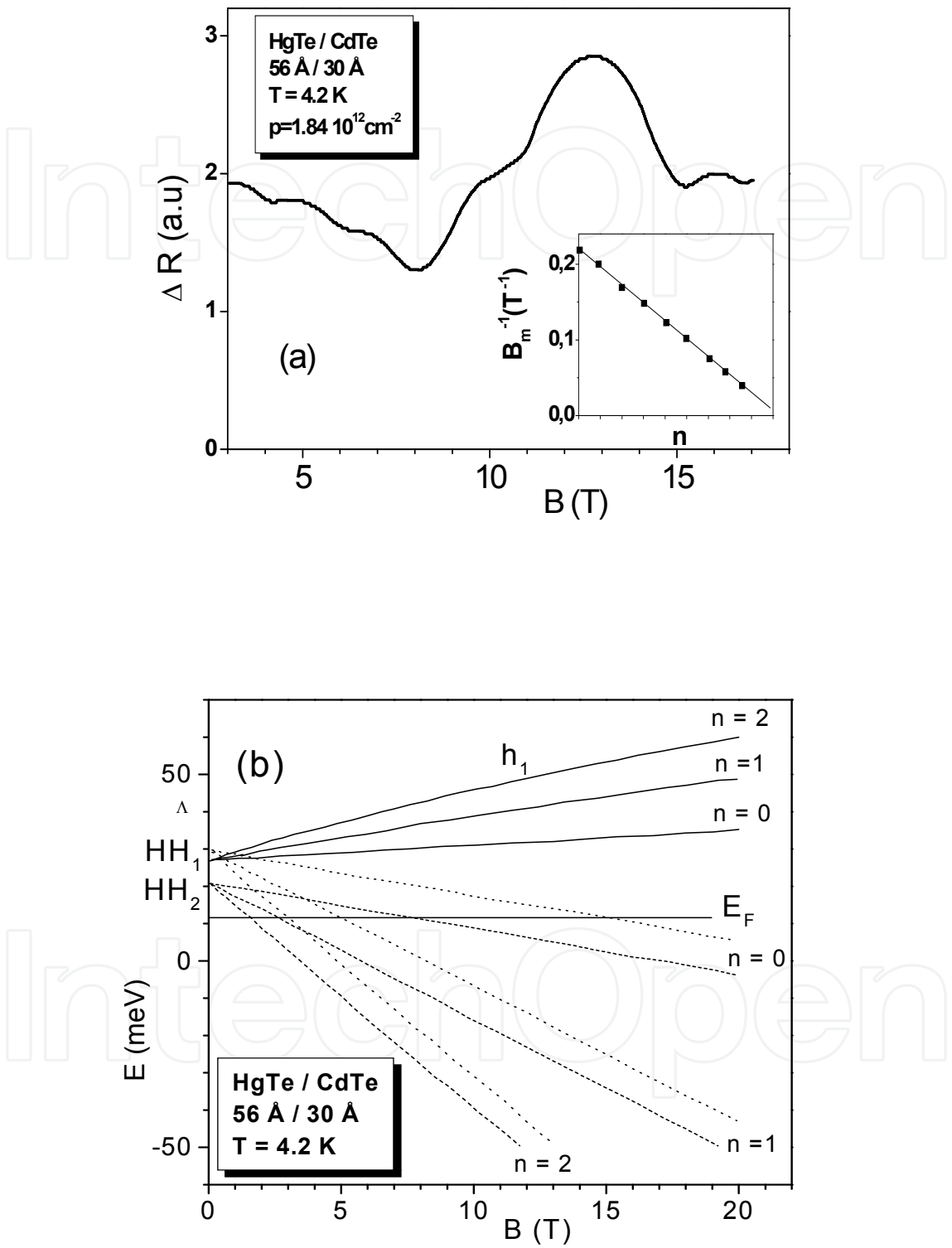
Band Structure and Magneto- Transport Properties in II-VI Nanostructures
Semiconductors. Application to Infrared Detector Superlattices

291

Fig. 6. (a) Variation of transverse magnetoresistance, with magnetic field of HgTe/CdTe superlattice, at 4.2 K (b) calculated Landau levels as a function of applied magnetic field of the HgTe/CdTe SL at 4,2 K. E_F is the Fermi level energy

and/or to the overlap between involved carriers sub-bands (HH$_1$) and (h$_1$) at (k$_z$, k$_p$) = (0, 0.008 Å^{-1}) and (π/d, 0.023 Å^{-1}) along E(k$_p$) in Fig. 4. Only the later cross over at E$_F$ can be taking into account. This increases the concentration p of holes (decreases of R$_H$ (1/T) in Fig. 5 (c)) and decreases of conductivity at 55 K (in Fig. 5 (d)) yielding to a decrease of mobility (in Fig. 5 (b)) due to the increase of effective mass from m$_{h1}$ to m$_{HH1}$. In intrinsic regime (245 K ≤ T ≤ 300 K), the measure of the slope of the curve R$_H$ T$^{3/2}$ indicates a gap E$_g$=E$_1$-E$_{HH1}$= 190 meV witch agree well with calculated E$_g$ (Γ, 300 K) =178 meV.

This relatively high mobility μ_p = 8200 cm²/Vs allowed us to observe the Shubnikov-de Haas effect (SDH) until 17 Tesla in Fig. 5. (a) (Nafidi et al, 2006). Its well knows that, for a two dimensional electronic gas, the oscillations of the magnetoresistance is periodic with respect to 1/B. The period Δ(1/B) is related to the concentration p of the holes by the relation:

$$p = \frac{e}{\pi \hbar \Delta\left(\frac{1}{B}\right)} \tag{8}$$

In the insert of Fig. 6(a) we have plot the inverse of the minima's 1/B$_m$ as a function of the entire n following the formula:

$$\frac{1}{B_m} = \Delta\left(\frac{1}{B}\right)\left(n + \frac{1}{2}\right) \tag{9}$$

The linear line slope gives Δ(1/B) =0.027 T^{-1} and p = 1.80 x 10^{12} cm^{-2} (in good agreement with 1.84x10^{12} cm^{-2} of weak field Hall effect from Fig. 5 (c)).

At low temperature, the superlattice heavy holes dominate the conduction in plane (Fig 4). The HH$_1$ (and h$_1$) band is parabolic with respect to k$_p$² (from Fig. 4). That permits us to estimate effectives masses $m^*_{HH_1}$ =0.297 m$_0$, $m^*_{h_1}$ =0.122 m$_0$ and the Fermi energy (2D) at 4.2 K

$$\left|E_F - E_{HH_1}\right| = \left|\frac{p \pi \hbar^2}{m^*_{HH_1}}\right| = 14 \text{ meV} \tag{10}$$

Around the (222) Bragg reflection in Fig. 7(a), a series of steps are observed corresponding to the oscillating counterparts described by (Arch et al, 1986). The difference with our results comes from the monocromacity and the power of their synchrotron source. Our SL1 is a modulated structure with high quality of interfaces.

The thermoelectric power α measurements shown in Fig. 6(b) (Nafidi et al, 2006) indicate a p-type conductivity, confirmed by Hall effect measurements in Fig. 5(c). At low temperature, $\alpha \sim T^{0.8}$ (in the top insert of Fig. 7(b)) is in agreement with Seebeck effect theory deduced from the relaxation time resolution of the Boltzmann equation (Seeger, 2002). For our degenerate holes gas the Seebeck constant is described by the formula:

$$\alpha = \frac{\left[(\pi k_B)^2 T (s+1)\right]}{3eE_F} \tag{11}$$

Band Structure and Magneto- Transport Properties in II-VI Nanostructures
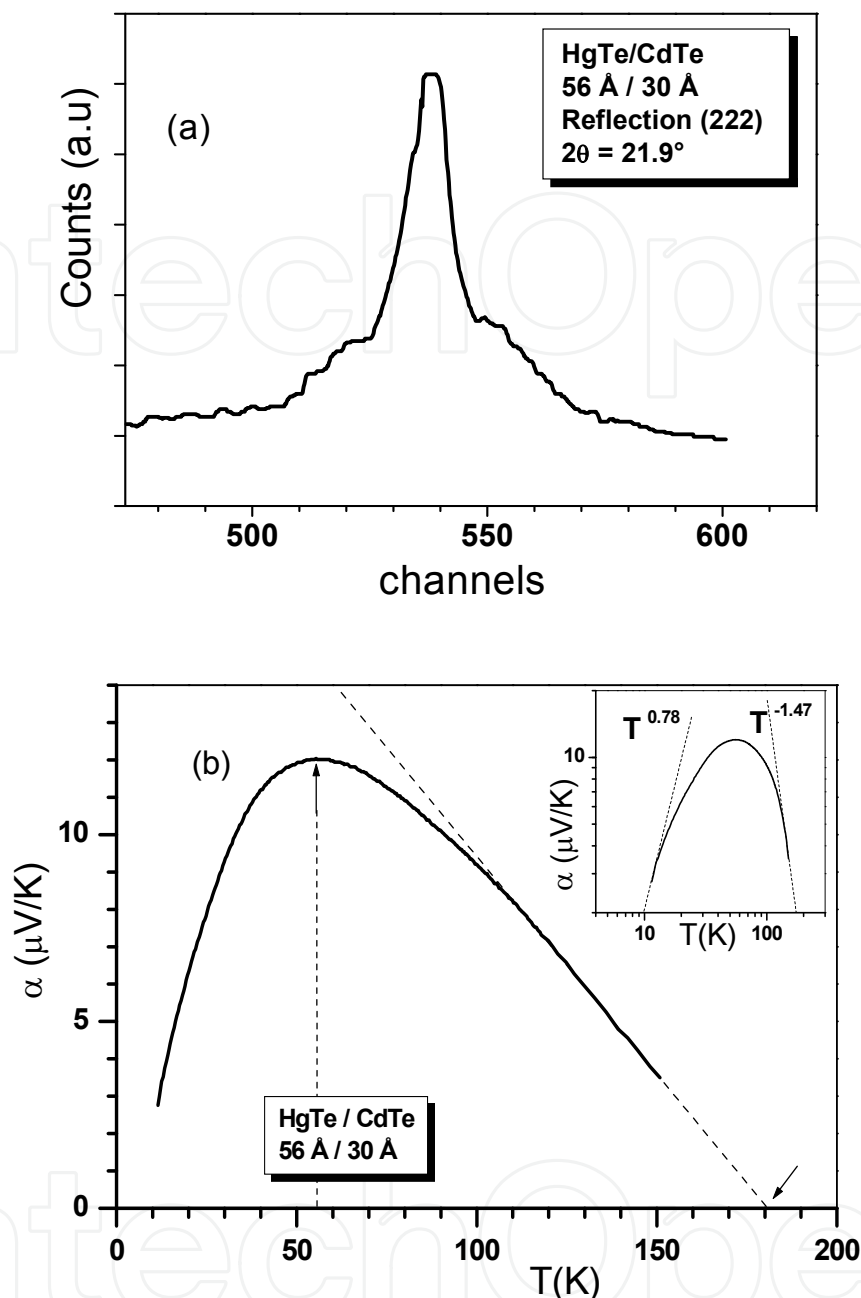Semiconductors. Application to Infrared Detector Superlattices

293

Fig. 7. (a) Room temperature X-ray diffraction profile around the (222) Bragg reflection of the HgTe/CdTe SL. (b) Measured thermoelectric power as a function of temperature of the HgTe/CdTe superlattice

and the collision time $\tau \sim E^{s-(1/2)}$. This permits us to estimate the Fermi energy at $E_F = 12$ meV (in Fig. 6(b)) in agreement with the calculated $|E_F-E_{HH1}|=14$ meV with s= 2.06 corresponding to holes diffusion by ionized impurities. It is relevant here to signal that the maximum of α at T=55.2 K correspond to the shift of Hall mobility in Fig. 5(b). Here $\mu_{HH1}= 2.434$ μ_{h1} at E_F. At T=190 K, a reversal of α sign will occur corresponding exactly to the minimum of the conductivity σ_0 in Fig. 5(d). From p = 1.80×10^{12} cm^{-2} of SDH we have deduced the effective masse of the degenerate heavy holes to be

$$m^*_{HH_1} = \frac{\pi p \hbar^2}{E_F} = 0.308\,m_0 \qquad (12)$$

(in agreement with the theoretical m*$_{HH1}$=0.297 m$_0$). We calculated the energy of the Landau levels (LL) by transposing the quantification rule of the wave vector in the plane of the SL:

$$k_p^2 = \frac{(2n+1)eB}{\hbar} \qquad (13)$$

where n are the quantum orders of LL. The crossing of E$_F$ with LL in Fig. 6(b) indicated the same magnetic field positions as those of the observed SDH oscillations minima B$_m$ in Fig. 6(a).

This HgTe/CdTe superlattice is a stable alternative for application in medium infrared optoelectronic devices than the random alloys Hg$_{0.8}$Cd$_{0.2}$Te because the small composition x=0.22, with E$_g$ (Γ, 300 K) =183 meV given by the empiric formula for Hg$_{1-x}$Cd$_x$Te (Hansen et al, 1982).

$$E_g(x,T) = -0{,}302 + 1{,}93x - 0{,}810x^2 + 0{,}832x^3 + 5{,}035 \times 10^{-4}(1\text{-}2x)\,T \qquad (14)$$

is difficult to obtain with precision while growing the ternary alloys and the transverse effective masse in superlattice is two orders higher than in the alloy. Thus the tunnel length is small in the superlattice (A. Nafidi et al, 2011).

5. The SL2: HgTe(d$_1$=18 nm) / CdTe(d$_2$= 4.4 nm)

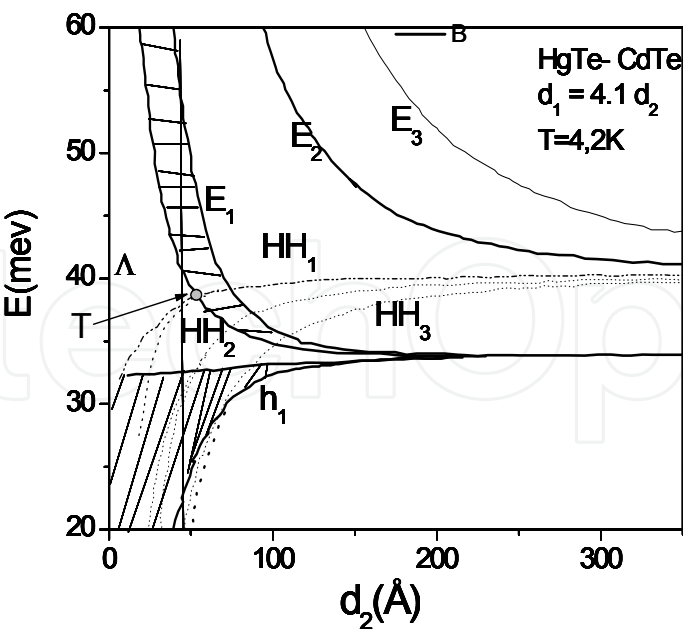### 5.1 Theoretical results and discussions

Fig. 8. Energy position and width of the conduction (E$_n$), heavy-hole (HH$_n$), and the first light-hole (h$_1$) subbands calculated at 4.2 K in the center Γ of the first Brillion zone as a function of layer thickness d$_2$ for HgTe/CdTe superlattice with d$_1$ = 4.1 d$_2$. T is the point of the transition semiconductor- semimetal

Band Structure and Magneto- Transport Properties in II-VI Nanostructures
Semiconductors. Application to Infrared Detector Superlattices

295

The energy E as a function of d_2, at 4.2 K, in the center Γ of the first Brillion zone and for $d_1 = 4.1\ d_2$, is shown in Fig. 8. The case of our sample ($d_2 = 44$Å) is indicated by the vertical solid line. Here the cross-over of E_1 and HH_1 subbands occurs. d_2 controls the superlattice band gap Eg = E_1-HH_1. For weak d_2 the sample is semiconductor with a strong coupling between the HgTe wells. At the point T(d_2 = 53.7 Å, E= 38.7 meV) the gap goes to zero with the transition semiconductor- semimetal. When d_2 increases, E_1 and h_1 states drops in the energy gap [0, Λ] and become interface state with energy E_I=34 meV for infinite d_2. Then the superlattice has the tendency to become a layer group of isolated HgTe wells and thus assumes a semimetallic character. The ratio d_1/d_2 governs the width of superlattice subbands (i.e. the electron effective mass). A big d_1/d_2, as in our case, moves away the material from the two-dimensional behavior.
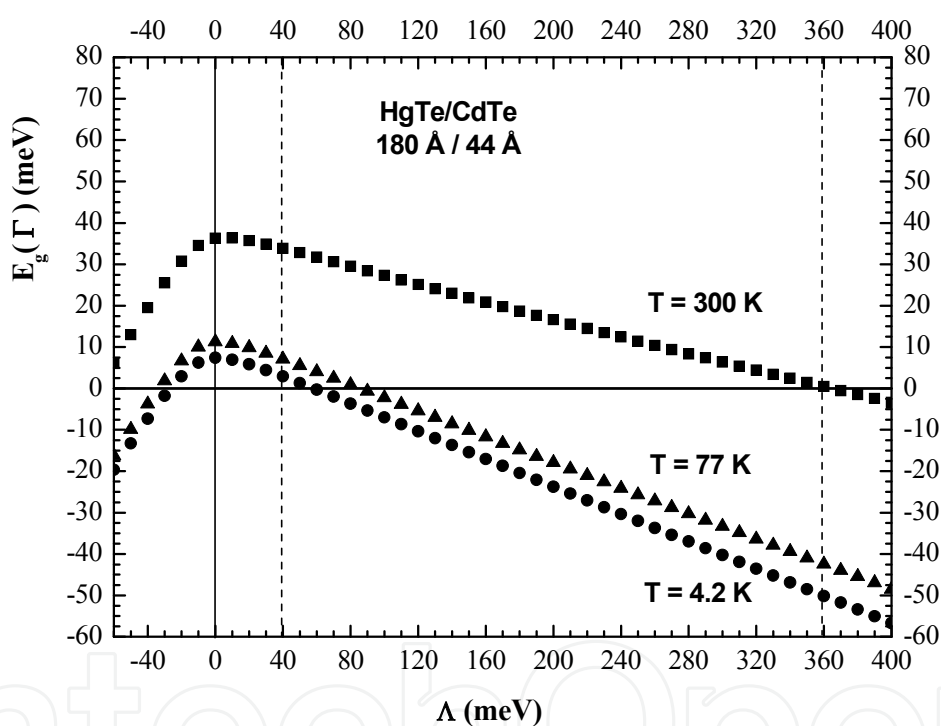

Fig. 9. The band gap E_g (Γ), at the center Γ of the first Brillion zone, as function of temperature and valence band offset Λ between heavy holes bands edges of HgTe and CdTe for the investigated HgTe/CdTe superlattice

In Fig. 9 we can see that the band gap $E_g(\Gamma)$ increases, presents a maximum at 0 meV and decreases when the valence band offset Λ between heavy hole band edges of HgTe and CdTe increase. For each Λ, $E_g(\Gamma)$ increases with T. Our chosen value of 40 meV is indicated by a vertical dashed line. This offset agrees well with our experimental results contrary to 0 meV used by (Bastard, 1982) and 360 meV given by (Johnson et al, 1988). The later offset give a zero gap whereas, in intrinsic regime, our measured E_g = 38 meV agree with calculated $E_g(\Gamma, 300\ K)$ = 34 meV.
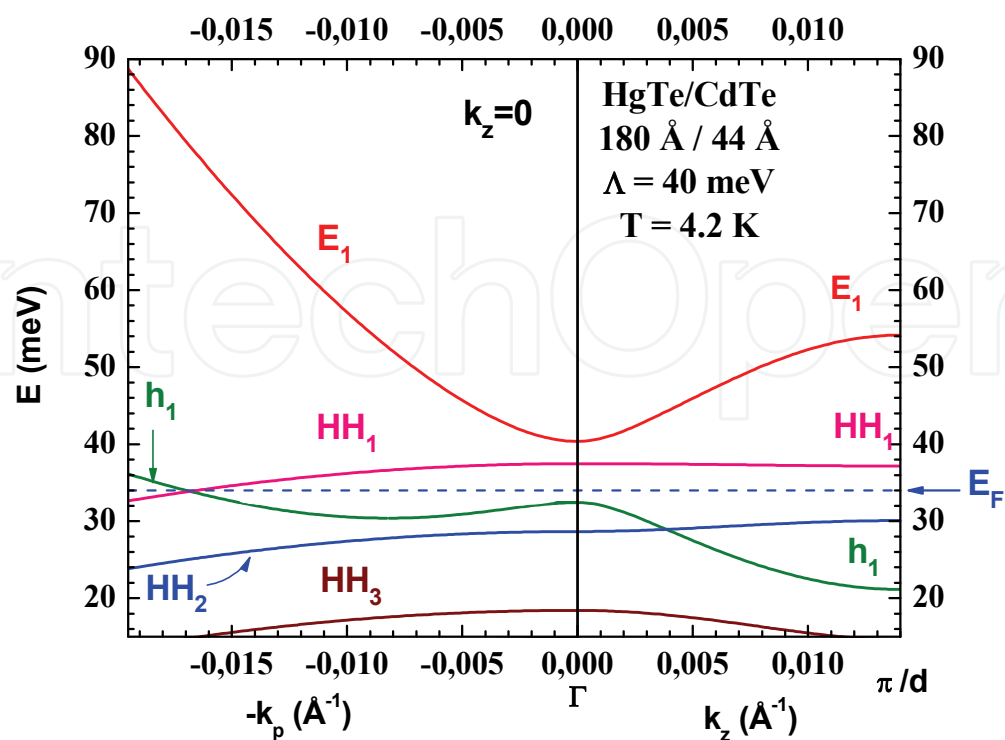
Fig. 10. Calculated bands along the wave vector k_z (a) and in plane $k_p(k_x,k_y)$ (b), of the HgTe/CdTe superlattice at 4.2 K. E_F is the energy of Fermi level
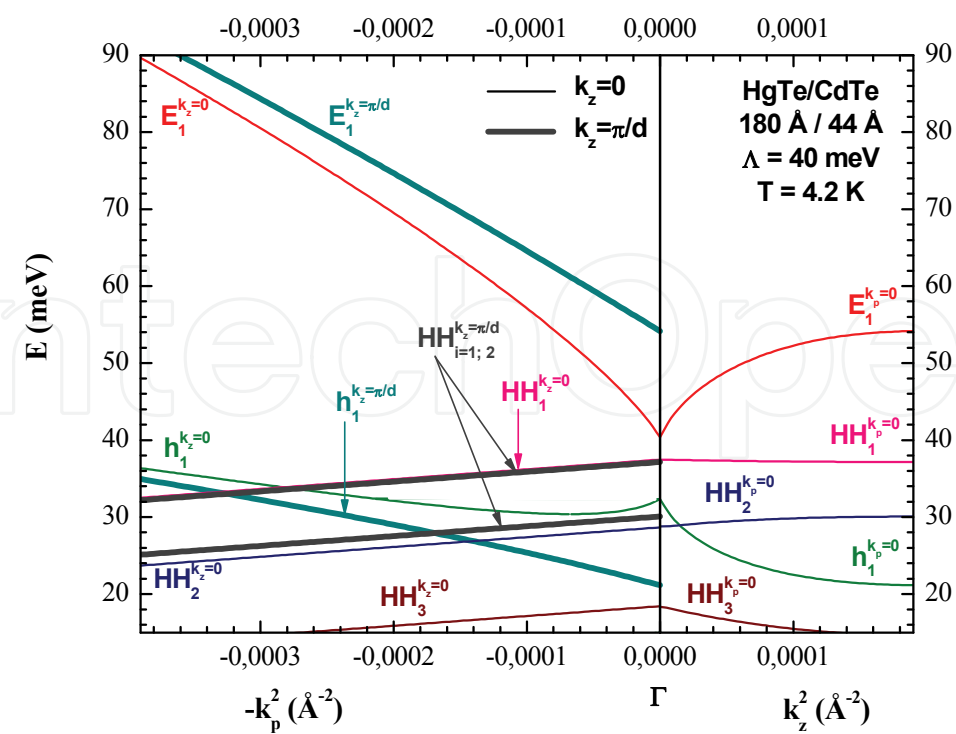

Fig. 11. Calculated bands as a function of k_z^2 and k_p^2 of the HgTe/CdTe superlattice at 4.2 K
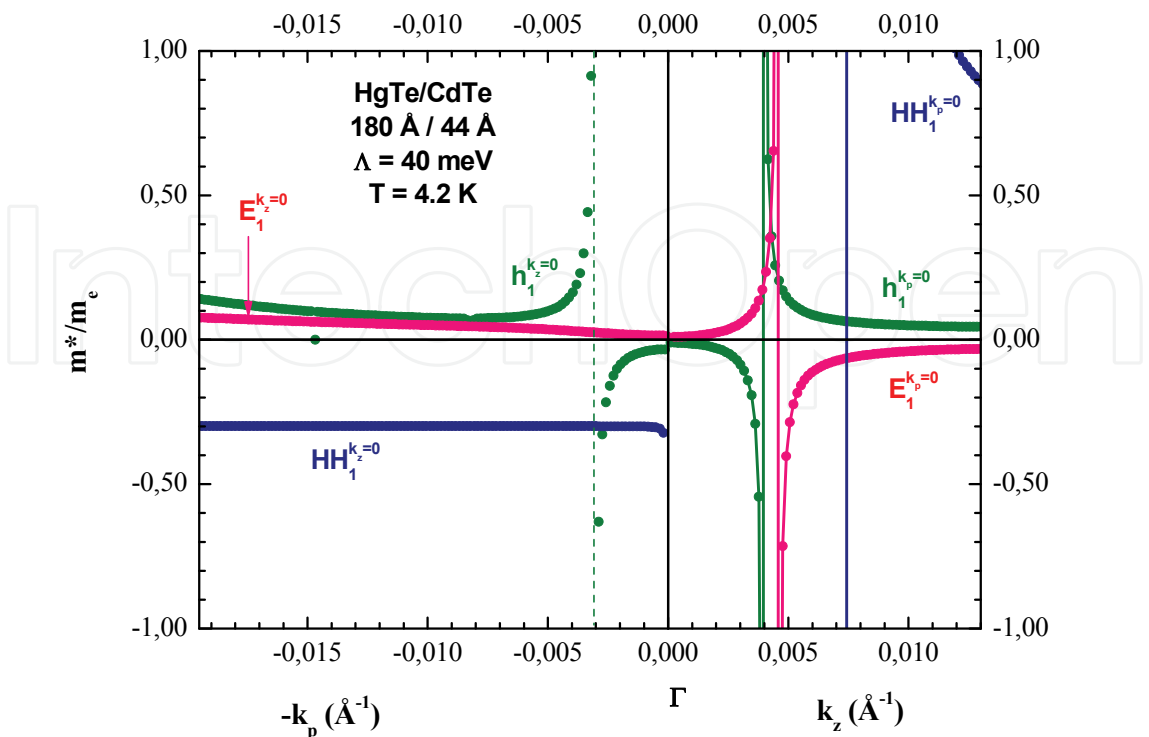
Band Structure and Magneto- Transport Properties in II-VI Nanostructures
Semiconductors. Application to Infrared Detector Superlattices

297

Fig. 12. Calculated relative effective mass bands along the wave vector k_z and in plane k_p of the HgTe/CdTe superlattice at 4.2 K

Fig. 10. show the spectra of energy $E(k_z)$ and $E(k_p)$, respectively, in the direction of growth and in plane of the superlattice at 4.2 K. Along $E(k_p)$, E_1 and h_1 increase with k_p whereas HH_n decreases. This yields to a anti-crossing of HH_1 and h_1 at $k_p=0.0168$ Å^{-1}. The gap is $E_g(\Gamma,4.2$ K$) = 3$ meV. Note that $E_F(4.2$ K$) =34$ meV$= E_I$ and then the conduction is assumed by heavy and light holes. As seen in Fig. 11., along k_z and k_p the light particles (electrons and light holes) subbands are not parabolic whereas the heavy hole subbands are parabolic.

For an anisotropic medium, such as the HgTe/CdTe superlattices, the effective mass is a tensor and its elements along μ and ν directions are given by the following expression [Kittel, 2001]:

$$\left(\frac{1}{m^*}\right)_{\mu\nu} = \frac{1}{\hbar^2}\frac{\partial^2 E_{k_{\mu\nu}}}{\partial k_\mu \partial k_\nu} \tag{15}$$

By carrying out second derivative of the energy E_1, h_1 and HH_1 along k_z and k_p in Fig. 10 we calculated the effective mass bands in Fig. 12. Along k_p, the effective mass of heavy holes $m^*_{HH1}= -0.300$ m_0 and the effective mass of electrons m^*_{E1} increases from 0.011 m_0 to 0.080 m_0 whereas the effective mass of the light holes h_1 deceases from 0.140 m_0 by half to a minimum of 0.074 m_0. After it increases and diverges at $k_p = 0.003$ Å^{-1} assuming a electronic conduction. After it increases to -0.034 m^0 at the center Γ of the first Brillion zone assuming a light hole conduction.

Using the same procedure as for the SL1 we get the temperature dependence of the band gap E_g, in the center Γ of the first Brillouin zone in Fig. 13. Note that E_g increases from 3.6

meV at 4.2 K to 34 meV at 300 K. In the investigated temperature range, the detection cut-off wave length verify : $40\,\mu m \leq \lambda_c \leq 500\,\mu m$. This situates our sample as a far infrared detector.
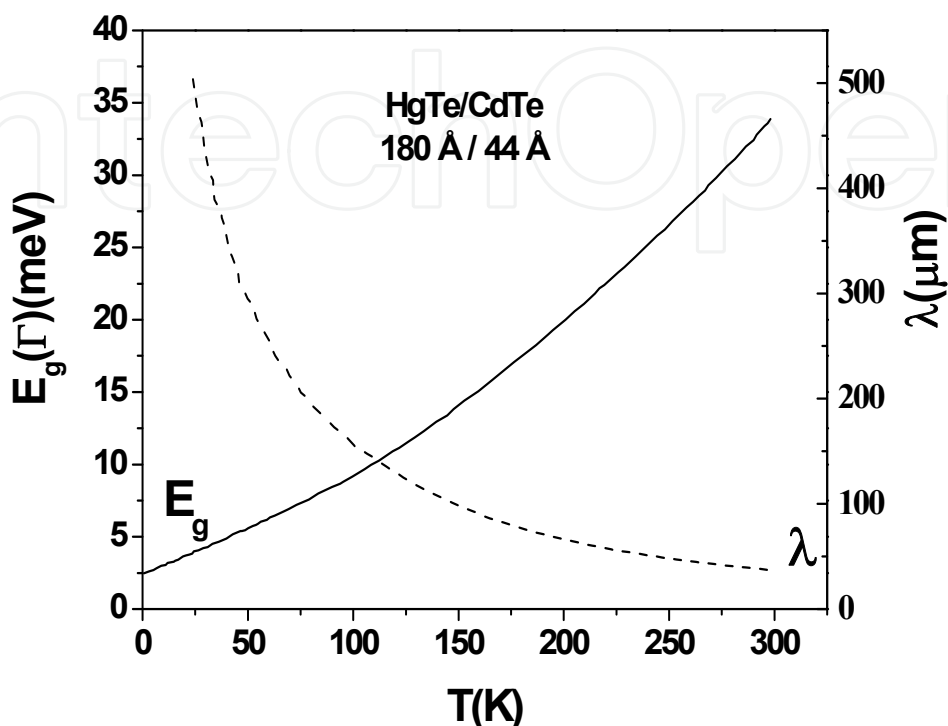

Fig. 13. Temperature dependence of the band gap E_g and cut-off wavelength, at the center Γ of the first Brillion zone, in the investigated HgTe/CdTe superlattice

5.2 Experimental results and discussions

The transverse magnetoresistance ρ/ρ_0, in Fig. 14, follows the two-dimensional (2D) dependence with manifestation of the beginning of the Shubnikov-de Haas oscillations (with a weak [$(\Delta \rho/\rho_0)max$ =0.2]). However, over the entire investigated magnetic field range, a non-vanishing magnetoresistance is observed when the field is parallel to the plane. This can be due to the inter-diffusion between HgTe well (big d_1/d_2 and small d_2) and/or to the widening of carriers subbands under the influence of the magnetic field along $E(k_P)$. While the Hall voltage V_H goes to zero at this configuration in Fig. 15. This suggests quasi two-dimensional conductivity behavior (between three-dimensional (3D) and two-dimensional (2D).

At low temperature, the sample exhibits p type conductivity with a hole mobility $\mu_p \approx 900$ cm²/V.s. As seen in Fig. 16 (b), a reversal of the sign of the weak-field Hall constant R_H occurs at 25 K. It may be attributed to trapping of carrier charges in intrinsic state E_I. Such a reversal of the sign of the Hall voltage may be inferred by the existence of at least two types of carriers, which suggests a semimetallic character of the conduction mechanism.

Fallowing the relaxation time resolution of the Boltzmann equation (Seeger b, 2002) (Kittel, 2001) the Hall constant at weak magnetic field in Fig. 16 (b) is described by the well knows formula:

$$(R_H)_w = \frac{1}{|e|} \frac{p-nb^2}{(p+nb)^2} \quad \text{with} \quad b = \frac{\mu_n}{\mu_p} \tag{16}$$

At low temperature in the saturation regime:

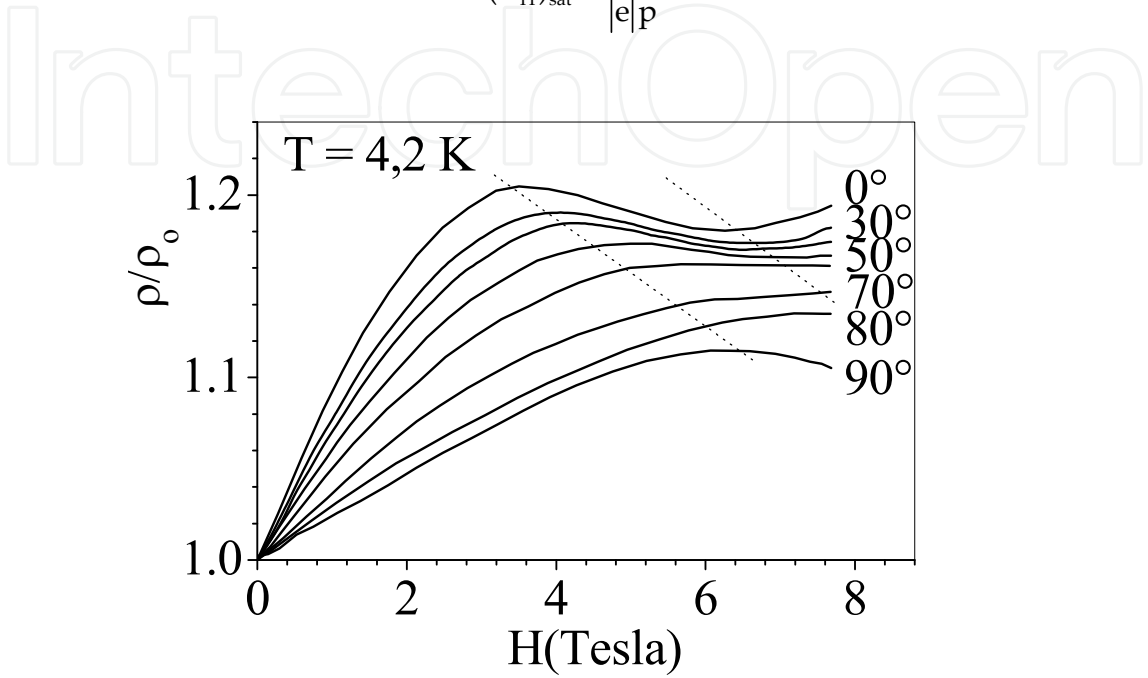$$(R_H)_{sat} = \frac{1}{|e|p} \tag{17}$$

Fig. 14. Transverse magnetoresistance of the sample, at various angles between the magnetic field and the normal to the HgTe/CdTe superlattice surface, at 4.2 K
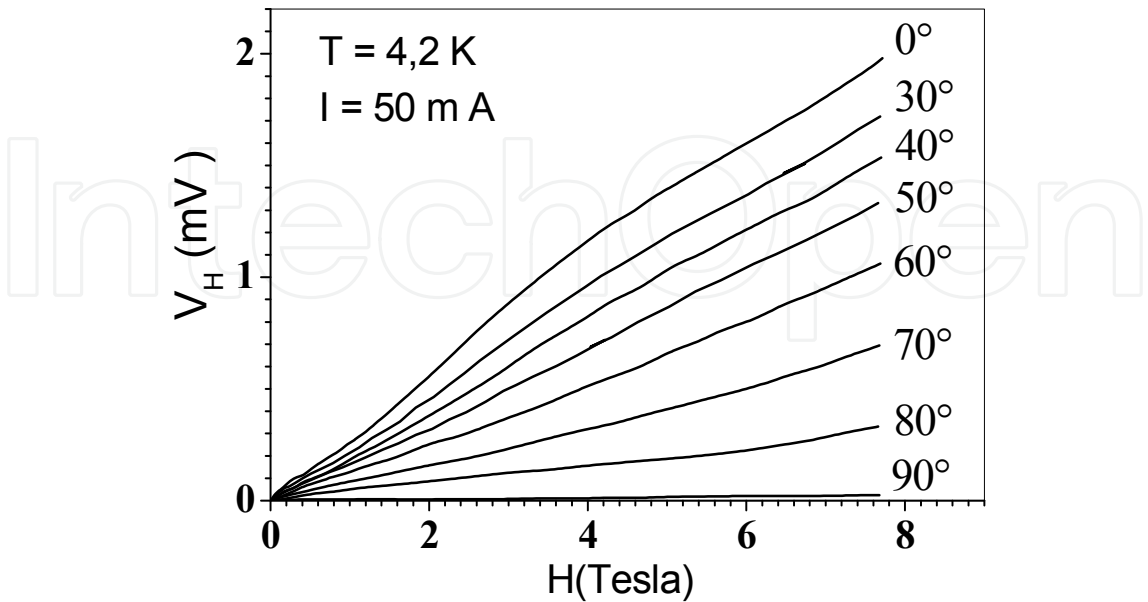

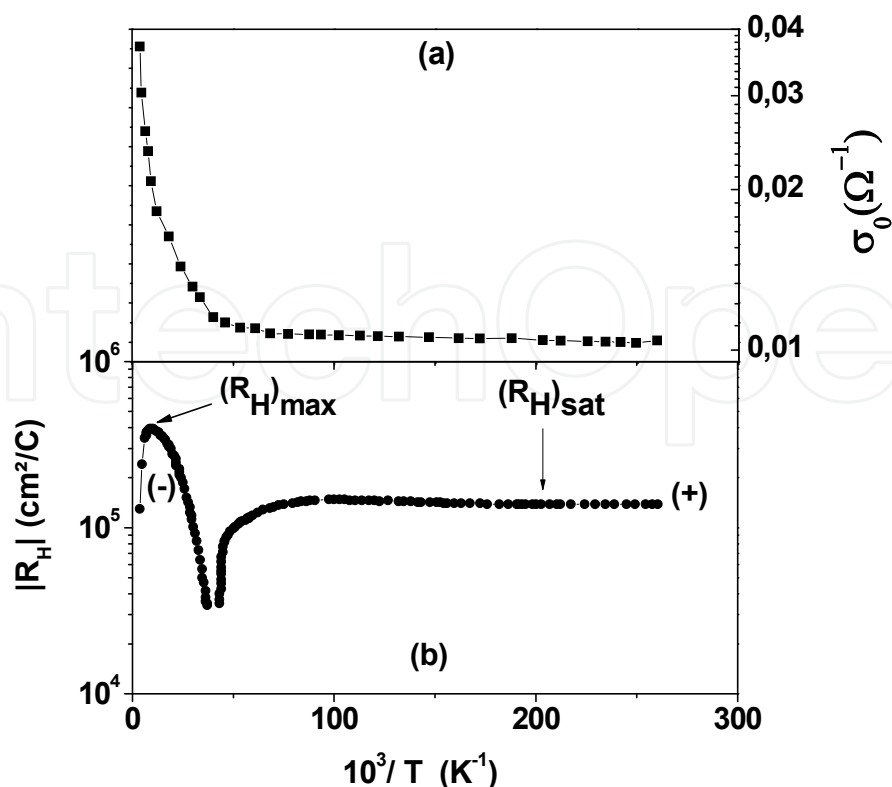Fig. 15. Field dependence of Hall voltage, at various angles between the magnetic field and the normal to the HgTe/CdTe superlattice surface, at 4.2 K

Fig. 16. Temperature dependence of the conductivity (a) and weak-field Hall coefficient (b), in the investigated HgTe/CdTe superlattice

Near the intrinsic regime, the maximum of the Hall constant is given by:

$$(R_H)_{max} = \frac{(b-1)^2}{|e|4bp} \tag{18}$$

This results in the ratio:

$$\frac{4(R_H)_{max}}{(R_H)_{sat}} = \frac{(b-1)^2}{b} \approx b = 32 \tag{19}$$

Eq. (15) implies for $R_H = 0$:

$$b^2 = 1024 = \frac{p}{n} \tag{20}$$

This implies an electron mobility of $\mu_n=3\times10^4$ cm²/V.s. Such a low value of the electron mobility can be connected, from the one side, with the superlattice electron effective mass which is much higher than that of the bulk material (Nafidi et al, 2011) and, from the other side, with different types of imperfections of the investigated structures, including strong compensation.

From Eq. (3) we have:

$$\frac{2}{3}P²\hbar²k_F^2 = E_F(E_F - E_g) \tag{21}$$

Band Structure and Magneto- Transport Properties in II-VI Nanostructures
Semiconductors. Application to Infrared Detector Superlattices

301

We extract the Fermi level energy:

$$E_F = \frac{E_g}{2} \pm \sqrt{\left(\frac{E_g}{2}\right)^2 + \frac{2}{3}P^2\hbar^2 k_F^2} \qquad (22)$$

Where the Fermi wave vector is $k_F(3D) = \left(3\pi^2 p\right)^{1/3}$ and $k_F(2D) = \left(2\pi p\right)^{1/2}$, respectively for three-dimensional and two-dimensional motion of carriers charges. Here we have chosen the minus sign because the sample is p-type at low temperature. Fig. 10 shows that the band gap and the 3D Fermi level energy increase with temperature whereas 2D Fermi level energy and HH_i bands energy remain constant. In all cases the conductivity is assumed by light and heavy holes. So we have quasi-two-dimensional and semimetallic conductivity. In table1 bellow we summarized the electronic transport parameters in the investigated two superlattices.
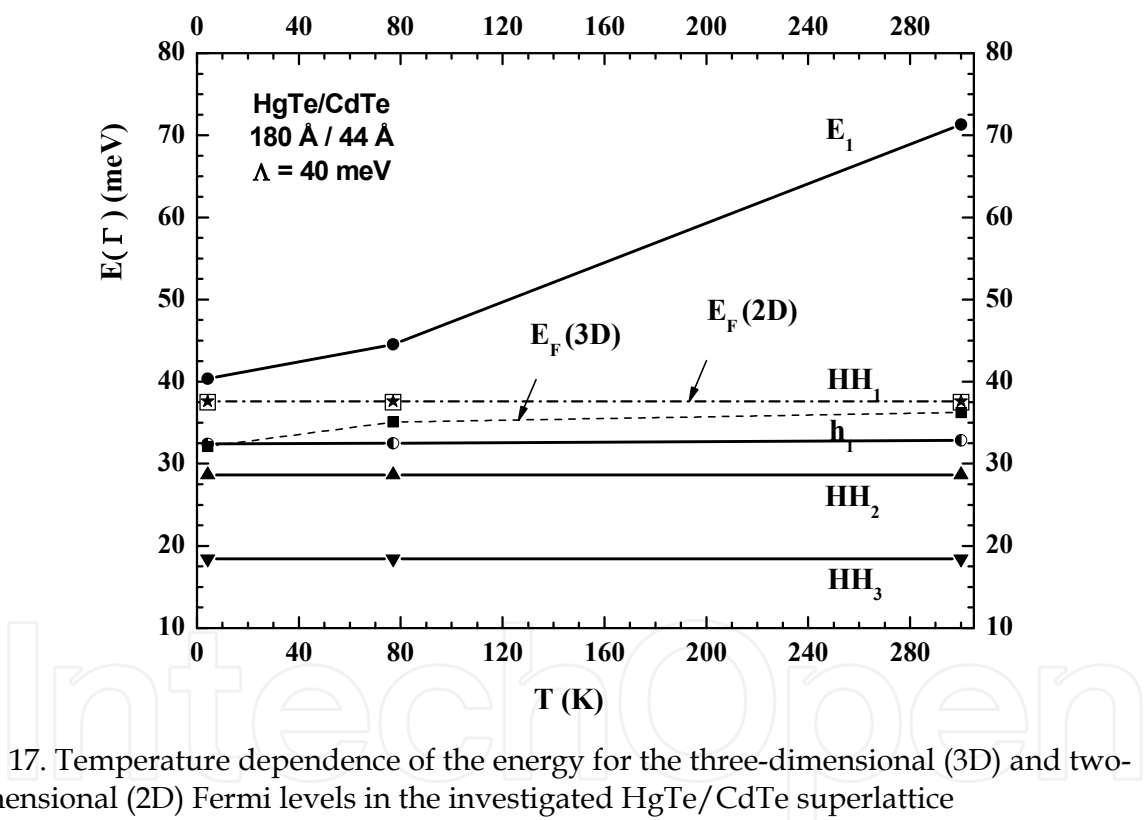

Fig. 17. Temperature dependence of the energy for the three-dimensional (3D) and two-dimensional (2D) Fermi levels in the investigated HgTe/CdTe superlattice

	E_g (meV) Theory 4.2 K	λ_c (μm) Theory 4.2 K	E_F(meV) Exper. 4.2 K	p (cm^{-2}) Hall ef. 4.2K	μ_P (cm^2/Vs) Hall ef. 4.2K
SL1 (p-type)	111	11 (MIR)	14 (2D)	1.84x10^{12}	8200
SL2 (p-type)	3.6	464 (FIR)	32 (3D) 38 (2D)	4.51x10^{13}	900

Table 1. Electronic transport parameters in the investigated two HgTe/CdTe superlattices

7. Conclusions

The fundamental main ideas of this work are:
- HgTe is a zero gap semiconductor (or semimetal) when it is sandwiched between the wide gap semiconductor CdTe (1.6 eV at 4.2 K) layers yield to a narrow gap HgTe/CdTe superlattice which is the key of an infrared detector.
- Before growing our two superlattices, we calculated the bands structures $E(d_2)$ and the gap for each ratio thickness d_1/d_2. After we choose the SL1 in the semiconductor conductivity zone and the SL2 at the transition semiconductor-semimetal

We reported here remarkable correlations between calculated bands structures and magneto-transport properties in two HgTe/CdTe nanostructures superlattices SLi (i=1 and 2). Our calculations of the specters of energy $E(d_2)$, $E(k_z)$ and $E(k_p)$, respectively, in the direction of growth and in plane of the superlattice; were performed in the envelope function formalism.

In the SL1, the formalism predicts that the system is semiconductor, for our HgTe to CdTe thickness ratio $d_1/d_2 = 1.87$, when $d_2 < 14$ nm. In our case, d_2=3 nm and E_g (Γ, 4.2 K) = 111 meV. In spite of it, the sample exhibits the features typical for the semiconductor type p conduction mechanism. In the used temperature range, this simple is a medium-infrared detector, narrow gap and two-dimensional p-type semiconductor.

In the SL2, the formalism predicts that the system is semimetallic, for our HgTe to CdTe thickness ratio d_1/d_2 =4.1 for $d_2 \geq 3$ nm. In our case d_2 = 4.4 nm and the gap $E_g(\Gamma,4.2$ K) =3 meV corresponding to thermal energy necessary to change the sign of $R_H(T)$. In intrinsic regime, the measurements indicates $E_g \approx 38$ meV in good agreement with calculated E_g (Γ, 300 K) =34 meV = E_F (4.2 K)=E_I. In spite of it, the sample exhibits the features typical for the semimetallic conduction mechanism, which agree well with the overlap between carrier subbands along $E(k_p)$ with a quasi-two-dimensional behavior and is a far-infrared detector.

Our HgTe/CdTe superlattices SL1 and SL2 are a stable alternative for application in infrared optoelectronic devices than the alloys $Hg_{0.8}Cd_{0.2}Te$ and $Hg_{0.66}Cd_{0.34}Te$ respectively. The theoretical and magnetotransport parameters are in good agreement. Measurements performed by us on others' samples indicate an improvement of quality of the material manifested by higher mobility.

8. Acknowledgements

9. References

Arch, D. K.; Faurie, J. P.; Staudenmann, J.L.; Hibbs-Brenner, M. & Chow, P. (1986). Interdiffusion in HgTe–CdTe superlattices. *J. Vac. Sci. Technol. A*, Vol, 4, (1986) (2101-2106), DOI: 10.1116/1.574035.

Bastard, G. (1981). Superlattice band structure in the envelope-function approximation. *Phys. Rev. B*, Vol,24, (November15, 1981) (5693–5697), DOI: 10.1103/PhysRevB.24.5693.

Bastard, G. (1982). Theoretical investigations of superlattice band structure in the envelope-function approximation. *Phys. Rev. B*, Vol, 25, (June 15, 1982) (7584–7597), DOI: 10.1103/PhysRevB.24.5693.

Band Structure and Magneto- Transport Properties in II-VI Nanostructures
Semiconductors. Application to Infrared Detector Superlattices

303

Cava, R. J. *Science* 247, pp. 656-662 (1990).

Dingle, R.; Gossard, A. C.; & Wiegmann, W. (1975). Direct Observation of Superlattice Formation in a Semiconductor Heterostructure. *Phys. Rev. Lett.*, Vol, 34, (May 26, 1975) (1327–1330), DOI:10.1103/PhysRevLett.34.1327.

El Abidi, A.; Nafidi, A.; Chaib, H.; El Kaaouachi, A.; Braigue, M.; Morghi, R.; EL Yakoubi, E.Y. & M. d'Astuto, (2010). Application of the transition semiconductor semimetal in modulated nanostructures for communication as infrared optoelectronic device. *Physica B: Physics of Condensed Matter*, Vol, 405, (1 February 2010) (936-940), DOI:10.1016/j.physb.2009.10.019 .

Esaki, L. & Tsu, R. (1970). Superlattice and negative differential conductivity in Semiconductors. *IBM J. Res. Development*, Vol., 14, (Jan. 1970) (61-65), ISSN: 0018-8646.

Guldner, Y.; Bastard, G.; Vieren, J.P.; Voos, M.; Faurie, J.P. & Million, A. (1984). Magneto-optics in a II–VI superlattice: HgTe-CdTe. *Surface Science*, Vol., 142, (1 July 1984) (593-597), DOI:10.1016/0039-6028(84)90367-4

Hansen, G. L.; Schmit, J. L. & Casselman, T. N., (1982).Energy gap versus alloy composition and temperature in $Hg_{1-x}Cd_xTe$. *J. Appl. Phys*, Vol., 53, (10 June 1982) (7099-7101), DOI:10.1063/1.330018.

Johnson, N. F.; Hui, P. M. & Ehrenreich, H. (1988). Valence-Band-Offset Controversy in HgTe/CdTe Superlattices: A Possible Resolution. *Phys. Rev. Lett.*, Vol, 61, (24 October 1988) (1993–1995), DOI: 10.1103/PhysRevLett.61.1993

Kane, E. (1957). Band structure of indium antimonide. *Journal of Physics and Chemistry of Solids*, Vol. 1, Issue 4,(January 1957) (249-261). DOI: 10.1016/0022-3697(57)90013-6

Kittel, C. (2001). *Introduction to solid stat physics*, 3d edition, John Wiley and Sons, Inc, New York, 333.

Nafidi, Ab.; El Kaaouachi, A.; Sahsah, H.; Nafidi, Ah. (2002). Band structure and magneto-transport in HgTe/CdTe superlattice. *Book of the International Conference on Theoretical Physics (HT 2002)*, pp. 274-275, ISBN 3-7643-2433-3, , 22-27 July, Paris, France Birkhäuser Verlag, Germany.

Nafidi, A.; El Kaaouachi, A.; Nafidi, Ah.; Faurie, J.P.; Million, A.; Piaguet, J. (2002). Some Transport Properties of HgTe/CdTe Superlattices. *Physica status solidi (b)*, Vol. 229, (January 2002) (573-576), DOI: 10.1002/1521.

Nafidi, Ab.; EL Abidi, A.; El Kaaouachi, A.; & Nafidi, Ah. (2004). Electronic Band Structure and New Magneto-transport Properties in p-type Semiconductor Medium-infrared HgTe / CdTe Superlattice. *27th International Conference on the Physics of Semiconductors - ICPS-27, AIP Conference Proceedings*, Vol. 772, pp. 1001-1002, DOI:10.1063/1.1994448, July 26-30, 2004, in Flagstaff, Arizona, USA.

Nafidi, A.; El Abidi, A. & El Kaaouachi, A. (2006). Seebeck and Shubnikov-de Haas Effects in a Two-Dimensional p-type HgTe/CdTe Superlattice. *24th International Conference on Low Temperature Physics - LT24 , AIP Conference Proceedings* Vol. 850,pp. 1359-1360, ISBN: 0735403473, 10 - 17 Aug 2005, Orlando, FL, USA.

Nafidi A., Bouallal A., El Kaaouachi B., A. and Chaib, H., *IEEE Transactions on Applied Superconductivity*. Vol 17 , NO 02, pp 2969-2972, (2007).

Nafidi A., Bouallal B., El Kaaouachi A., Chaib H. and Sahsah H., Advance in Cryogenic Engineering, *Transactions of the International Cryogenic Materials conference-ICMC*, American Institute of Physics, AIP CP986, Vol.54, pp.551-558, (2008).

Nafidi, A., et al, (2011) to be published

Sakaki, H.; Chang, L. L.; Sai-Halasz, G. A.; Chang, C. A. & Esaki, L. (1978). Two-dimensional electronic structure in InAs-GaSb superlattices. *Solid State Communications*, Vol. 26, (June 1978) (589-592), DOI:10.1016/0038-1098(78)90770-6

Seeger, K. a (2002). *Semiconductor physics: an introduction,* Springer, ISBN: 9783540438137, Edition Number: 8, chap.4, p.121.

Seeger, K. b (2002). *Semiconductor physics: an introduction,* Springer, ISBN: 9783540438137, Edition Number: 8, chap.6, p.159.

Tokura, Y. Takagi, H and Uchida, S. *Nature* 337, pp. 345-347 (1989).

Tuchendler, J.; Grynberg, M.; Couder, Y.; Thomé, H. & Le Toullec R. (1973). Submillimeter Cyclotron Resonance and Related Phenomena in HgTe. *Phys. Rev. B,* Vol., 8, (15 October 1973) (3884–3894), DOI: 10.1103/PhysRevB.8.3884.

Weiler, M. H. (1981). Magnetooptical Properties of Hg1-xCdxTe Alloys, In: *semiconductors and Semimetals*, Vol., 16, Willardson, R. K. & Beer, A. C. (Ed), (119-191) (Academic, New York), ISBN: 9780127521169
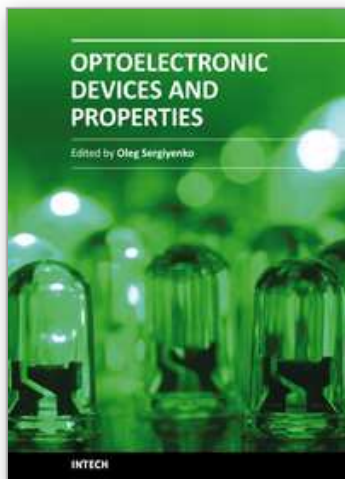
Optoelectronic Devices and Properties

Edited by Prof. Oleg Sergiyenko

ISBN 978-953-307-204-3

Hard cover, 660 pages

Publisher InTech

Published online 19, April, 2011

Published in print edition April, 2011

Optoelectronic devices impact many areas of society, from simple household appliances and multimedia systems to communications, computing, spatial scanning, optical monitoring, 3D measurements and medical instruments. This is the most complete book about optoelectromechanic systems and semiconductor optoelectronic devices; it provides an accessible, well-organized overview of optoelectronic devices and properties that emphasizes basic principles.

How to reference

In order to correctly reference this scholarly work, feel free to copy and paste the following:

INTECH

open science | open minds